EFFECT OF BLADE-ALIGNED CASING TREATMENT SLOTS ON PERFORMANCE OF A TRANSONIC COMPRESSOR ROTOR.

***Abstract*:**

Aerodynamic stall caused by shock-triggered tip leakage vortex (TLV)decay severely restricts the operating margin of transonic axial compressors and accelerates stall onset. To alleviate this boundary layer phenomenon, three-dimensional steady Reynolds-Averaged Navier-Stokes (RANS) computations were performed on an isolated NASA Rotor 37 geometry to evaluate passive flow mitigation using blade-aligned, over-tip casing slots. Performance on a standard smooth shroud was benchmarked against three slot configurations varying in depth 3mm, 4 mm, and 5) while maintaining a fixed width of 3mm and length of 56.5 mm, using a validated multi-block structured mesh (1.22 10^6 elements). The 3 mm slot depth variant (CT_1) expanded the stall margin by 2.3 through bleeding high-pressure fluid near the trailing edge and reinjecting it ahead of the passage shock to prevent vortex breakdown. Entropy visualizations indicate thatinternal cavity recirculation generates shear-driven thermal dissipation, incurring a modest peak efficiency penalty across all slotted models. While matching slot geometry with tip camber effectively suppresses end wall flow blockage, controlling cavity volume remains essential to limit internal mixing losses.

Keywords: Transonic axial compressor, NASA Rotor 37, Blade-aligned casing treatment, Tip leakage vortex, Shock-vortex interaction, Stall margin extension, k"-" ϵ turbulence model, Passive flow control.

Introduction: -

Running modern axial compressor stages at transonic relative speeds boosts pressure loading and overall power-to-weight ratios in gas turbine powerplants. However, these high Mach regimes introduce intricate aerodynamic structures within the blade tip clearance gap. Driven by the static pressure difference between the blade pressure and suction surfaces, fluid escaping across the narrow tip gap rolls into a concentrated Tip Leakage Vortex (TLV).

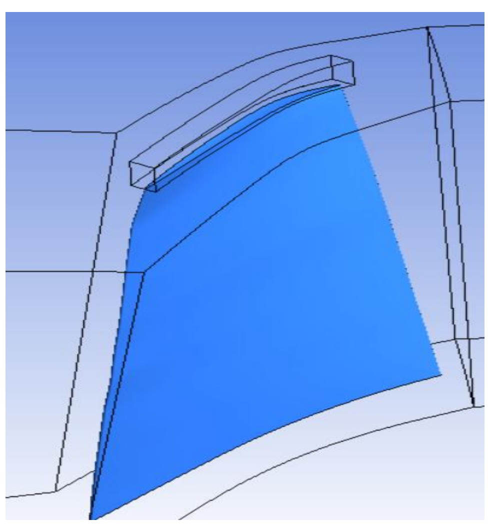

Figure 1.Casing Treatment Over Blade Tip

In transonic rotors like NASA Rotor 37, this leakage flow directly intersects the passage shock wave adjacent to the outer casing shroud. As mass flow decreases toward stall, severe shock-vortex interactions trigger vortex core breakdown. The resulting low-momentum stagnation bubble migrates upstream toward the leading edge, eventually spilling into neighboring passages and initiating rotating stall or full compressor surge. To mitigate tip region instabilities and broaden operating boundaries, passive casing modifications have been widely investigated. Early foundational work established that endwall blockage generated by tip clearance flows dominates stage losses and defines stability thresholds. Subsequent flow control designssuch as circumferential grooves, axial skewed slots, and recirculating cavities—aimed to interrupt this leakage flow mechanism. Studies demonstrated that circumferential grooves enhance operating stability mainly by altering axial momentum balance across the tip gap, though performance remains sensitive to clearance height. Self-recirculating concepts further proved that extracting high-pressure air near the rear chord and reinjecting it upstream of the shock energizes the endwall boundary layer. Nevertheless, unoptimized slot cavities frequently generate internal shear mixing, causing noticeable efficiency penalties near peak operating points. Despite extensive research on standard slot and groove geometries, finding a casing modification that provides meaningful stall margin expansion without unacceptable efficiency loss remains a persistent engineering challenge. Most prior studies focused on basic axial or circumferential configurations, leaving a gap in understanding how over-tip slots contoured precisely along the local blade camber line influence shock-vortex breakdown mechanics. To address this gap, the present work investigates the aerodynamic impact of blade-aligned casing treatment slots applied over the tip shroud of an isolated NASA Rotor 37. Aligning the slot contour with local blade stagger and camber across the mid-to-rear chord directly taps into the intrinsic pressure differential across the tip gap. Three-dimensional steady RANS simulations using a validated structured grid (1.22 10^6) evaluate flow field development, pressure ratio recovery, and entropy generation across the operating map. The baseline smooth shroud is benchmarked against three slot height variations (3mm, 4 mm, and 5 mm) to determine the optimal balance between stability enhancement and parasitic slot mixing losses.

Literature Review

Aerodynamic stall caused by shock-triggered tip leakage vortex decay severely restricts the operating margin of transonic axial compressors and accelerates stall onset (Nejad & Taghavi-Zenouz, 2024). To address these stability constraints, secondary flows originating from tip clearance interactions exacerbate adverse pressure gradients, thereby intensifying the formation and subsequent breakdown of these vortices (Endo et al., 2025a, 2025b). Passive casing treatments, such as axial slots, have emerged as a viable intervention to suppress these flow instabilities by redistributing aerodynamic loading and alleviating end-wall blockage (Beheshti et al., 2004; Yu.D. et al., 2021). These configurations improve stability by re-energizing the low-momentum fluid within the tip region, which effectively delays the onset of surge (Shivaramaiah et al., 2025; Wilke & Kau, 2004). Although these treatments successfully extend the stall margin, they often necessitate a trade-off in peak adiabatic efficiency due to increased mixing and recirculating energy losses (Vuong & Kim, 2021; Zhang et al., 2020). Recent investigations demonstrate that these efficiency deficits arise from primary entropy generation at the leading edge and secondary dissipation concentrated near the slot trailing edges (Chi et al., 2025). To mitigate such performance penalties, researchers have explored hybrid designs, such as coupling axial slots with circumferential grooves to re-energize leakage flow and minimize tip-region blockages at near-stall conditions (Zhu & Yang, 2020). Optimizing the meridional profiles of these configurations through surrogate-based modeling further enables the identification of geometry parameters that maximize stability while simultaneously constraining efficiency degradation (Ba, Du, et al., 2024; Ba, Fan, et al., 2024). The identification and elimination of such near-casing blockage, which typically manifests downstream of the tip leading edge where the passage shock interacts with the leakage vortex, remains fundamental to enhancing the stability limits of high-pressure compressor stages (Mustaffa & Fikri, 2020). Consequently, the accurate quantification of this blockage parameter is essential for evaluating how variations in slot depth and cavity volume influence the interaction between the passage shock and the tip leakage flow (Mustaffa &Kanjirakkad, 2021).

Methodology

Overview of NASA Rotor 37

Engineered by the NASA Glenn Research Center in the late 1970s, NASA Rotor 37 remains an iconic, highly loaded transonic axial compressor stage. Although initially conceived as an inlet stage for advanced aircraft core compressors, it rapidly evolved into an indispensable aerodynamic benchmark. Today, turbomachnery researchers worldwide depend on this baseline geometry to validate computational fluid dynamics (CFD) solvers, calibrate high-fidelity turbulence closures, and unearth the complex flow physics governing high-speed internal aerodynamics.

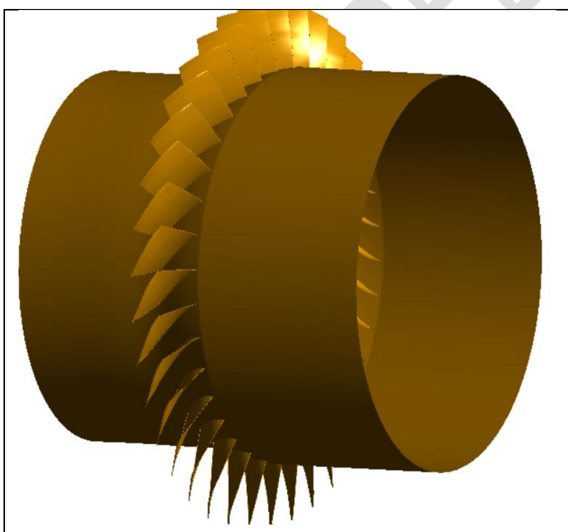

Figure .2 CAD 3-D Model of NACA Transonic Compressor Rotor

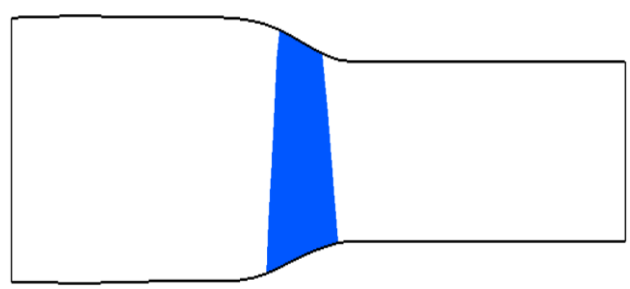

Figure.3 Meridional View of Rotor 37 Over Blade Path

Key Specifications for Rotor 37

SL NO	Parameters	Value
1	No of rotor Blades	36
2	**No of stator Blades**	36
3	**Design Mass Flow**	20.19 kg/s
4	**Choking Mass Flow**	20.93 kg/s
5	**Total Pressure Ratio**	2.106
6	**Total Temperature Ratio**	1.27
7	**Rotor tip speed**	454.136 m/s
8	**Aspect ratio**	1.19
9	**Tip solidity**	1.29
10	**Inlet Hub-To-Tip diameter ratio**	0.7
11	**Tip clearance**	0.356 mm
12	**Blade profile**	Multiple-Circular-Arc (MCA)

Geometric Modeling and Computational Flow Domain

By taking advantage of rotational symmetry allowed us to reduce the computational domain to a single blade passage rather than modeling the full 360° rotor assembly. This approach preserved the core passage aerodynamics while drastically cutting computational cost. The three-dimensional CAD model of the rotor blade was constructed in CATIA V5 R19, as illustrated in Fig. 3.

To prevent artificial acoustic reflections from contaminating the inner flow field during transonic operation, the domain boundary was extended upstream by two chord lengths (2C) and downstream by three chord lengths (3C). Extending the inlet plane gives the incoming flow sufficient distance to establish a uniform velocity profile prior to hitting the leading edge. Similarly, the downstream buffer zone provides ample space for trailing-edge wakes, tip leakage structures, and secondary passage flows to decay naturally before reaching the exit. Figure 3 presents the overall domain topology along with the applied boundary conditions: total inlet conditions, static exit pressure enforcing radial equilibrium, no-slip constraints on rotating and stationary walls, and periodic boundaries along the pitch wise faces.Spatial discretization was performed in ANSYS ICEM CFD using a structured multi-block hexahedral topology. We wrapped an O-grid around the airfoil contour to maintain high mesh orthogonality near the curved blade surface, while H-grid blocks populated the main passage core and domain extension zones. Aligning grid lines with the primary flow direction minimizes numerical cross-diffusion and cleanly resolves steep pressure gradients across passage shocks. To capture boundary layer dynamics directly without wall functions, the first cell height adjacent to all solid surfaces was restricted to maintain $y^{+}<5$. Element density was strategically refined in high-gradient regionsmost notably the leading edge, trailing edge, and tip clearance gapyielding the final discretized grid shown in Figure 4.

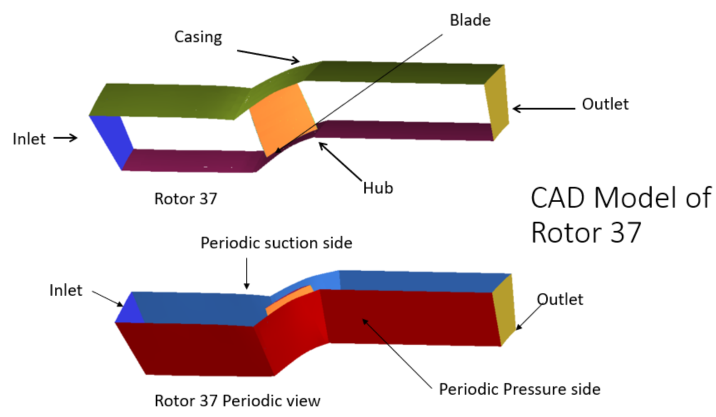

Figure 4. Computational Domain Comprising Rotor Blade Passage

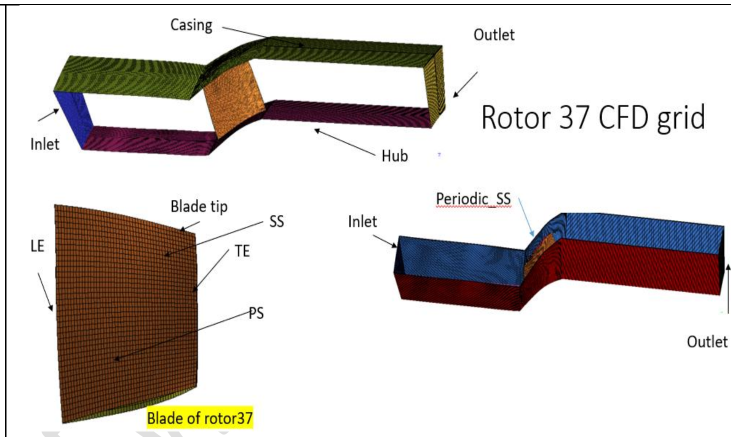

Figure.5 Discretized Computational Domain for Rotor Blade Passage

Numerical Solver and Turbulence Modeling

Numerical simulations were performed in ANSYS CFX to solve the three-dimensional, steady, compressible Reynolds-Averaged Navier-Stokes (RANS) equations. The solver employs a fully coupled, element-based finite volume scheme paired with a second-order high-resolution advection scheme, ensuring high spatial accuracy across steep pressure gradients and passage shock waves. Turbulence closure was achieved using the Shear Stress Transport (SST) k"--" ω turbulence model, which is widely favored in turbomachinery research for its reliability in predicting adverse pressure gradients and near-wall boundary layer behavior under low-Reynolds-number ($y^{+}<5$) conditions. To model frame rotation, the rotor blade and hub surfaces were defined in the rotating reference frame, whereas the stationary outer casing shroud was assigned a counter-rotating relative motion. No-slip conditions were enforced on all solid wall boundaries. At the computational inlet, uniform total pressure, total temperature (matching sea-level standard atmospheric conditions), and an axial flow direction were prescribed. Conversely, static pressure was specified across the exit boundary to control stage loading. Solution convergence was systematically tracked across all primitive variables, with final convergence declared once root-mean-square (RMS) residual values dropped below 10^{-5}

Grid Independence Study and Validation

To evaluate mesh sensitivity and establish spatial grid independence, numerical simulations were performed across three structured hexahedral grid densities (G1 with 0.6 million elements, G2 with 1.2 million elements, and G3 with 2.4 million elements) at 100% design speed. The compressor performance map was resolved from choke to near-stall conditions by incrementally increasing the exit static pressure. As depicted in the compressor performance curves, the total pressure ratio and isentropic efficiency predictions for G2 and G3 show strong asymptotic convergence, exhibiting virtually identical trends throughout the operating range. Specifically, both G2 and G3 predict a maximum total pressure ratio of approximately 2.07–2.08 at a corrected mass flow rate near 19.5 kg/s and a peak isentropic efficiency of roughly 86.6% around 20.9 kg/s, whereas the coarse mesh G1 under-predicts performance across all mass flow rates. Consequently, grid G2 with 1.2 million elements was chosen as the optimum mesh for further computations. In comparison with the experimental data, the CFD model accurately captures the vertical choke line at approximately 21.1 kg/s and closely reproduces the overall shape of the performance curves. However, the simulation slightly under-predicts the peak experimental pressure ratio (~2.15) and peak isentropic efficiency (~89.3%), and exhibits a narrower stall margin (stall initiation near 19.5 kg/s in CFD versus 19.4 kg/s in experiments). These minor discrepancies are primarily attributed to steady-state numerical assumptions that filter out unsteady shock-wave oscillations and tip vortex interactions, differences in boundary layer growth due to truncated computational duct lengths, and the assumption of uniform inlet flow profiles in the CFD setup as opposed to the spanwise total pressure and velocity gradients present in the experimental facility.

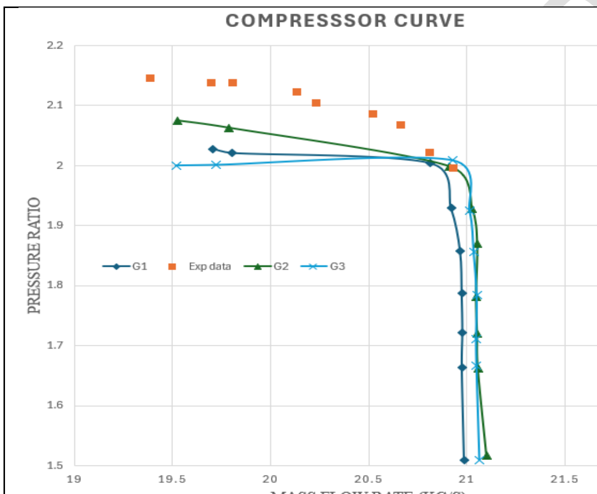

Figure.6 Grid Independence Study – Variation of Total Pressure Ratio with Mass Flow Rate

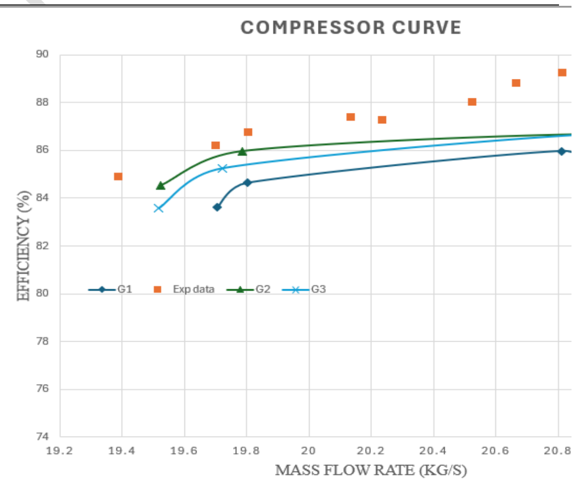

Figure.7 Grid Independence Study – Variation of Efficiency with Mass Flow Rate

Modeling of Compressor Stage with Casing Treatment Slots

Casing treatment performance is governed by several geometric variables, including slot count, pitch, aspect ratio, and depth. To systematically assess how mean camber line slots influence rotor aerodynamics, this initial study focuses on varying slot count and aspect ratio. Two distinct casing treatment configurations, designated CT-1, CT-2, CT-3 were modeled in CATIA V5 R19. Figure 7 illustrates the 3D CAD assembly for the CT-1 treated compressor stage, while Table 1 details the precise geometric parameters for both configurations.

Table 1: Design Specifications of Casing Treatment Slots

	Width (mm)	Height (mm)	Length (mm) Equal to blade ti
Case 1	3	3	56.5
Case 2	3	4	56.5
`Case 3	3	5	56.5

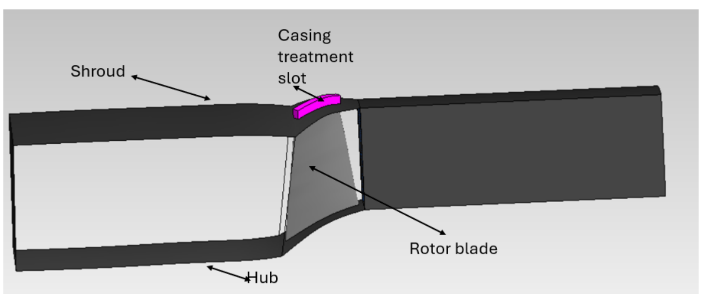

Figure 8: Compressor Rotor with Casing Treatment Slots

The domain topology, solver setup, and boundary conditions for the casing-treated models were kept consistent with the baseline smooth shroud configuration (1.22×10^6 cells) to ensure accurate comparative analysis. Additional structured hexahedral elements were generated inside the over-tip slot cavities to resolve internal recirculation, increasing the computational grid size to approximately 1.45"--" 1.52×10^6 cells across the treated cases. Figure 8 illustrates the discretized computational domain for the blade-aligned slot design, while Table 3 summarizes the exact element counts for the baseline and each slot width configuration.

Table 2: Computational Grid Size for Rotor with Casing Treatment Slots

Sl no	Computational grid	Num of Hexa cells in millon cells
1	Baseline rotor	1.2
2	Rotor with casing treatment slots	1.45

Results:

Effect of Casing Treatment Slot

Evaluating overall compressor maps demonstrates clear shifts in stage loading and stable operating limits when over-tip blade-aligned casing slots are introduced. For the baseline NASA Rotor 37, numerical predictions closely reproduce experimental choke mass flow rates near 21.1" kg/s". maintaining strong agreement along the vertical choke region while slightly under-predicting peak adiabatic efficiency. Across all three treated slot configurations (3" mm" 4" mm", and 5" mm" widths), the computational results indicate that integrating over-tip slots introduces an isentropic efficiency penalty across the entire operating range. Specifically, the 3" mm" slot design extends the stable mass flow boundary down to 19.12" kg/s" achieving a 2.3% stall margin improvement over the baseline smooth shroudyet its peak efficiency decreases from 86.7% to approximately 85.5%. Expanding the slot width to 4" mm" and 5" mm" causes further efficiency degradation down to roughly 84.5%, under-predicting performance in both the choke and near-stall operating regimes. This efficiency deficit stems primarily from internal cavity dynamics, where fluid bleeding through the rear portion of the slot undergoes severe shear mixing and viscous dissipation before re-entering the main passage stream ahead of the passage

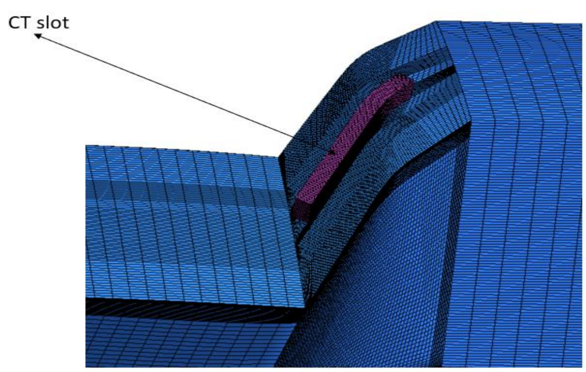

Figure 9: Computational Grid for Compressor Stage with Casing

shock.

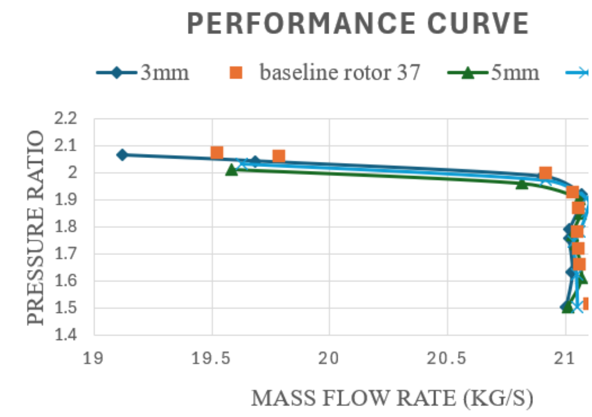

Figure.10 Variation of Total Pressure Ratio with Mass Flow Rate at Design Rotor Speed

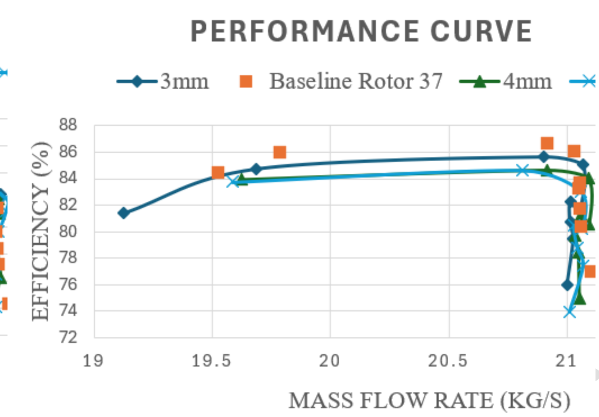

Figure. 11 Variation of Efficiency with Mass Flow Rate at Design Rotor Speed

Flow Field Visualization and Contour Analysis in Blade to Blade Passage

Mach Contour plot in blade-to-blade passage

Evaluating relative Mach number (M_"rel") distributions across the span under near-stall conditions illustrates the primary fluid dynamic mechanism behind stall margin extension. Flow velocity maps adjacent to the outer casing wall reveal clear topological shifts between the smooth shroud and the casing-treated configurations:

Baseline Rotor 37: Displays a pronounced, dark blue low-Mach stagnation bubble (M<0.2) along the suction surface (SS) near the leading edge. This stagnation bubble marks severe flow blockage resulting from the passage shock wave colliding with the Tip Leakage Vortex (TLV) core.

CT_1 Configuration (3" mm” Width): The low-Mach blockage core is largely eliminated and pushed downstream. Driven by cross-blade pressure differentials, the slot bleeds high-pressure endwall fluid near the trailing edge and reinject it upstream ahead of the shock wave. This high-velocity jet (red/orange contours, M>1.2) energizes the local boundary layer, delaying vortex breakdown and extending the stable mass flow limit down to 19.12" kg/s" (a 2.3% stall margin improvement).

CT_2 (4" mm") & CT_3 (5" mm") Configurations: Localized low-speed pockets reappear near the mid-chord region. This indicates that overly wide slot cavities disrupt mainstream momentum without yielding further aerodynamic stability gains.

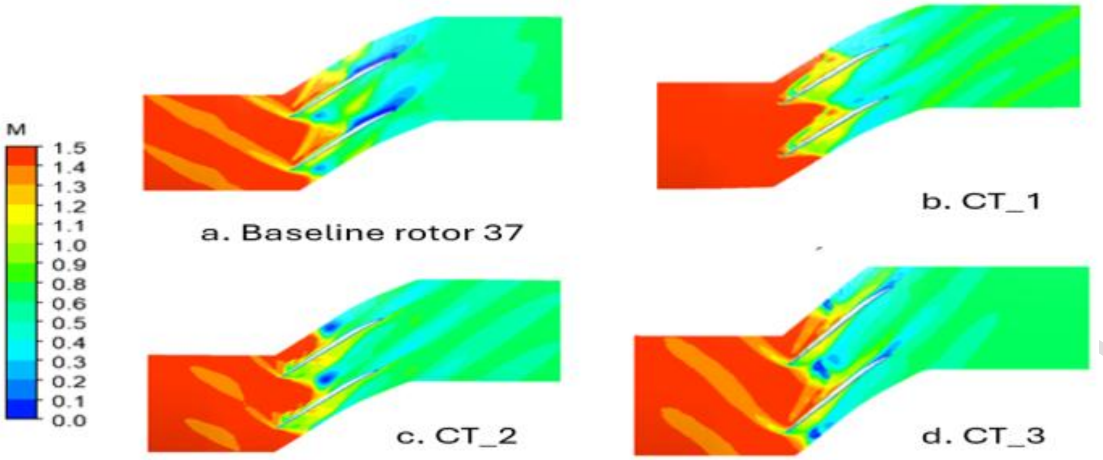

Figure 12.Mach Counter Plots at Stall Operating Point

Entropy Contour Plot in Blade to Blade Passage

To examine the thermodynamic losses introduced by the over-tip slots, relative entropy (s) distributions were evaluated across a constant-span blade-to-blade surface near the rotor tip (99% span). Comparing the baseline smooth shroud against the treated configurations highlights clear differences in loss patterns and flow behavior:

Baseline Rotor 37 (Smooth Shroud)

Loss Distribution: Shows a large, high-entropy zone ($150\text{--}200\ \mathrm{J \cdot kg^{-1} \cdot K^{-1}}$) that diffuses broadly across the mid-to-rear passage.

Flow Physics: Caused by the unmitigated breakdown of the Tip Leakage Vortex (TLV) as it collides with the passage shock, creating severe flow separation and blockage.

CT_1 Configuration (3 mm Slot Width)

Loss Distribution: Replaces the wide mid-passage loss cloud with narrow, tight entropy streaks confined directly along the slot contour.

Flow Physics: Continuous fluid bleed near the trailing edge and upstream reinjection prevent core vortex breakdown from spreading into the main flow.

Performance Impact: The compact 3 mm cavity keeps internal shear mixing low, limiting the peak adiabatic efficiency drop to 85.5% while yielding a 2.3% stall margin gain.

CT_2 Configuration (4 mm Slot Width)

Loss Distribution: High-entropy regions begin spreading outward along both the axial and circumferential directions near the rear chord.

Flow Physics: The wider 4 mm slot increases cavity volume, creating stronger internal recirculation loops that heighten viscous dissipation before the fluid re-enters the main passage.

CT_3 Configuration (5 mm Slot Width)

Loss Distribution: Produces a massive, high-entropy core spanning across the entire passage trailing edge.

Flow Physics: Excessive cavity volume triggers heavy internal turbulence and wall friction, causing the re-emerging air to act as a physical obstruction to the core stream.

Performance Impact: Causes the highest thermodynamic losses, dropping peak isentropic efficiency to $\approx 84.5\%$ with no added gain in stability.

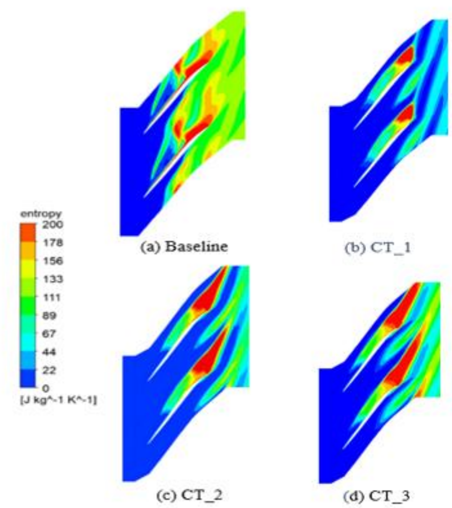

Figure 13.Entropy Contour for Peak Efficiency Point

Span Wise Flow Development at Rotor Exit

Specific Entropy Distributions at Rotor Exit (s, $J \cdot kg^{-1} \cdot K^{-1}$)

(a) Baseline Rotor 37 (Smooth Shroud)

Loss Topology: Thermodynamic loss is almost exclusively concentrated in the thin blade trailing edge wakes running vertically from hub to tip.

Endwall Losses: The entropy generation along the outer shroud remains low and tightly bounded to the immediate tip clearance gap.

(b) "CT_1" Configuration (3" mm" Slot Width)

Loss Topology: A distinct, high-entropy core (150"--" 200" J"·〖"kg" 〗^(-1)·"K" ^(-1), red region) appears near the outer shroud at the tip span.

End wall Losses: Because the 3" mm" slot cavity volume is small, this high-entropy region is kept compact and close to the casing wall, preserving low-entropy core flow across 85"--" 90% of the blade span.

(c) "CT_2" Configuration (4" mm" Slot Width)

Loss Topology: The red high-entropy core expands circumferentially across the upper passage shroud.

End wall Losses: The increased slot width fosters stronger internal shear mixing within the slot cavity, driving higher thermodynamic losses into the upper endwall flow.

(d) "CT_3" Configuration (5" mm" Slot Width)

Loss Topology: Displays the largest and most intense high-entropy red zone spanning across the entire top portion of the passage at the rotor exit.

End wall Losses: The large 5" mm" cavity acts as an internal turbulence generator, causing significant viscous dissipation that penetrates deep into the blade span and accounts for the lowest overall isentropic efficiency (≈84.5%).

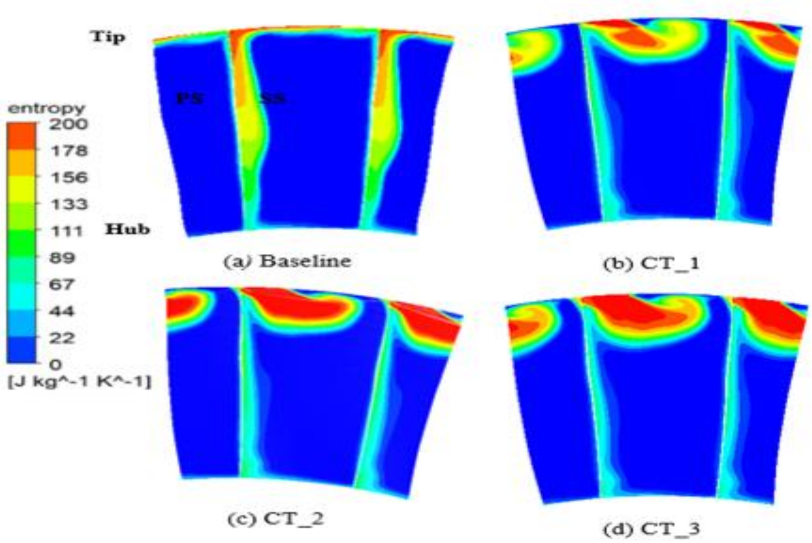

Figure 14Variation of Entropy at Stream Wise Plane-2 At Mass Flow Rate Equal to Stall Mass Flow Rate: (A) Baseline Stage, (B) Casing Treated Stage Case Ct-1, (C) Casing Treated Stage Case Ct-2 And (D) Casing Treated Stage Case Ct-3

Relative Mach contour (Plane-1 at Near Trailing Edge / Stall Region):

- Predominant Focus: Shows flow separation, blade boundary layer thickness, and trailing edge wake development.
- Baseline vs. Casing treatment:The baseline case shows a distinct low-velocity wake (blue/cyan stripe) clinging to the suction side (SS).

In the casing-treated cases (CT_1, CT_2, CT_3), the end wall flow is redistributed. However, localized low-momentum patches (blue spots) appear near the casing shroud because of the air bleeding into and out of the slot cavities.

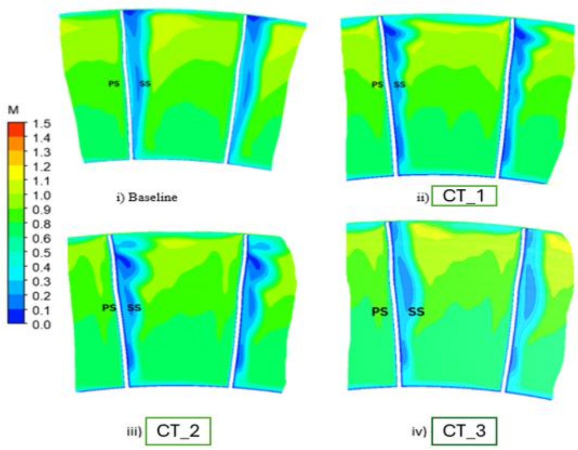

Figure 15 Variation of Relative Mach Number on Streamwise Plane-1 At Near Design Mass Flow Rate Of 20.188 Kg/S: (A) Baseline Stage, (B) Casing Treated Stage Case Ct-1, And (C) Casing Treated Stage Case Ct-2 And (D) Casing Treated Stage Case Ct-3

Second Plot Set (Plane-2 Downstream Exit / Core Flow):

- Predominant Focus: Shows overall passage mass flux, core flow energization, and end wall momentum deficit downstream.
- Baseline vs. Casing treatment:
- The baseline rotor exhibits a moderate velocity core across the span.
- The casing-treated cases show massive bright red high-momentum cores ($M_{\mathrm{rel}} > 1.2$) filling the main passage. This proves that the slot reinjection jet successfully energizes the primary passage flow downstream, even though a thin low-velocity boundary region (dark blue) forms right against the top outer shroud.

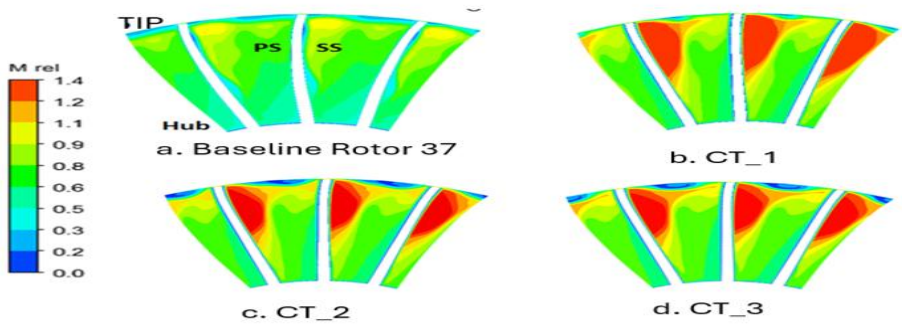

Figure.16 Variation of Relative Mach Number on Streamwise Plane-2 At Near Design Mass Flow Rate Of 20.188 Kg/S: (A) Baseline Stage, (B) Casing Treated Stage Case Ct-1, And (C) Casing Treated Stage Case Ct-2 And (D) Casing Treated Stage Case Ct-3

CFD Methodology Block Diagram Used in the Research

Figure.17: Stages of CFD Methodologies used in Research

Conclusions

The effect of over-tip blade-aligned casing treatment slots on the aerodynamic performance of a transonic axial compressor stage has been thoroughly investigated. Numerical simulations were carried out on a transonic compressor stage without and with three configurations of casing treatment. The overall stage performance and the secondary flow development through the blade passages were systematically examined across all models. The important conclusions derived from this study are:

Baseline rotor predictions agree well with published experimental data, capturing shock-vortex interactions with slight under-predictions in pressure ratio and efficiency. Casing treatment induces three-dimensional flow redistribution within the rotor passage across axial, tangential, and radial directions. The compressor stage with the CT_1 configuration 3mm depth, 3 mm width) demonstrates the optimal balance between stability and efficiency. It suppresses tip leakage vortex breakdown and expands the stall margin by 2.3%, while bounding the peak efficiency penalty to 85.5% due to its compact cavity volume. Configurations with deeper slots CT_2 and CT_3) display higher thermodynamic losses and reduced isentropic efficiency down to 84.5% approximately across the operating range due to larger cavity volumes fostering strong internal recirculatory eddies and shear mixing. Casing treatment slots directly influence end wall flow by bleeding high-pressure fluid near the trailing edge and reinjecting it upstream, effectively suppressing tip leakage flow formation and extending stall margin. Casing treatment plays a vital role in enhancing axial compressor stall marginimproving it by 2.3%thereby significantly expanding the stable operating range of gas turbine engine.

References

1. Chen, G.T. Greitzer, E.M. Tan, C.S. and Marble, F.E., (1991) “Similarity Analysis of Compressor Tip Clearance Flow Structure”, ASME Journal of Turbomachinery, Vol.113, pp. 260-271
2. Lakshminarayana B., Zaccaria M. and Marathe B., (1995) “The Structure of Tip Clearance Flow in Axial Flow Compressors”, ASME Journal of Turbo machinery, Vol.117.
3. Suder, K.L. and Celestina M.L., (1994) “Experimental and Computational Investigation of the Tip Clearance Flow in a Transonic Compressor Rotor”, NASA TM-106711, 1994.
4.] Copenhaver W. W., Mayhew E. R., Hah C. and Wadia A. R., (1996) “The Effect of Tip Clearance on a Swept Transonic Compressor Rotor”, ASME Journal of Turbo machinery, Vol.118.
5. Schwenk F. C. and G.W. Jr. Lewis, (1955) “Experimental investigation of a transonic axial-flow- compressor rotor with double-circular-arc airfoil blade sections: comparison of blade-element performance with three levels of solidity”ResearchMemorandumE55F01, NACA, Cleveland, Ohio, June 1955
6. W.A. Benser (1974) “Transonic Compressor Technology Advancement” Technical paper, NASA Lewis Research Center, USA, 1974
7. W.R. Britsch, W.M. Osborn, and M.R. Laessing (1979) “Effects of diffusion factor, aspect ratio and solidity on overall performance of 14 compressor middle stages” Technical paper 1523, NASA, Cleveland, Ohio, September 1979.
8. VassiliosPachidis,Pericles Pilidis, Ioannis Templalexis, Theodosios Alexander, and Petros Kotsiopoulos, (2006) “Predictions of Engine Performance Under Compressor Inlet Flow Distortion Using Streamline Curvature” GT2006-90806, ASME Turbo Expo 2006: Power for Land, Sea, and Air, May 8-11, 2006 ,Barcelona , Spain.
9. Hamzezade, M., AGHA, S. M. M., &Bazazzadeh, M. (2019). Numerical study of the effect of the tip gap size and using a single circumferential groove on the performance of a multistage compressor.
10. Brown, W. J. (2020). Experimental and Numerical Evaluation of the Performance of a High-Speed Centrifugal Compressor at Off-Design Conditions (Master's thesis, Purdue University).

11. Gibson, L., Spence, S., Kim, S. I., Schwitzke, M., & Starke, A. (2018, May). A numerical investigation of a turbocharger compressor back-disk cavity at widely varying operating conditions. In *Proceedings of the International Turbocharging Seminar* (Vol. 2018, p. 11).
12. Borgoltz, A. (2007). Modifications of coherent structures in fan blade wakes for broadband noise reduction.
13. Hancock, M. (2025). *Heat Transfer and Aerodynamic Losses Caused by Additively Manufactured Turbine Blades Enhanced by Micro-Machining and Chemical Polishing*. The University of Alabama in Huntsville.
14. Sidhu, S. S. (2024). PERFORMANCE INFLUENCE OF LEADING-EDGE TUBERCLES ON A HIGH-SPEED AXIAL COMPRESSOR.
15. Chi, C. (2022). *Aeromechanics of a Double Anhedral Tip Composite Rotor: Experiment and Modeling*. University of Maryland, College Park.
16. Zhang, Y., Li, Y., Bian, X., & Yuan, X. (2019). Effects of inlet swirl on pressure side film cooling of neighboring vane surface. *Journal of Thermal Science and Engineering Applications*, *11*(6), 061008.
17. Brown, D. K. S. (2026). *Strain Gage Preparation and Application Techniques For Aeroelastic Investigations on a Transonic Fan* (Doctoral dissertation, Purdue University Graduate School).